

# Journal of Materials Science & Technology

## Understanding the hydrogen effect on pop-in behavior of an equiatomic high-entropy alloy during in-situ nanoindentation

--Manuscript Draft--

|  |  |
|--|--|
| <b>Manuscript Number:</b>                            | J-MST-D-21-00421R1   |
| <b>Full Title:</b>                                   | Understanding the hydrogen effect on pop-in behavior of an equiatomic high-entropy alloy during in-situ nanoindentation  |
| <b>Short Title:</b>                                  |  |
| <b>Article Type:</b>                                 | Letter   |
| <b>Section/Category:</b>                             |  |
| <b>Keywords:</b>                                     | nanoindentation; Pop-in; hydrogen; Dislocation; High-entropy alloy   |
| <b>Corresponding Author:</b>                         | Xu Lu<br>Norges teknisk-naturvitenskapelige universitet<br>NORWAY  |
| <b>Corresponding Author Secondary Information:</b>   |  |
| <b>Corresponding Author's Institution:</b>           | Norges teknisk-naturvitenskapelige universitet   |
| <b>Corresponding Author's Secondary Institution:</b> |  |
| <b>First Author:</b>                                 | Dong Wang  |
| <b>First Author Secondary Information:</b>           |  |
| <b>Order of Authors:</b>                             | Dong Wang<br>Xu Lu<br>Meichao Lin<br>Di Wan<br>Zhiming Li<br>Jiaying He<br>Roy Johnsen   |
| <b>Order of Authors Secondary Information:</b>       |  |
| <b>Abstract:</b>                                     | <p>The variations in the pop-in behavior of an equiatomic CoCrFeMnNi high-entropy alloy under different hydrogen charging/discharging conditions were characterized via in-situ electrochemical nanoindentation. Results show that hydrogen accumulatively reduces both pop-in load and width, among which the reduction of pop-in width is more noticeable than that of pop-in load. Moreover, the hydrogen reduction effect on both pop-in load and width is reversible when hydrogen is degassed during anodic discharging process. Particularly, the hydrogen-reduced pop-in width was studied in detail by a comprehensive energy balance model. It is quantitatively shown that the dissolved hydrogen enhances lattice friction, leading to an increased resistance to dislocation motion. As a result, fewer dislocations can be generated with a higher hydrogen concentration, causing a smaller pop-in width. This is the first time that the pop-in width indicated dislocation mobility under hydrogen impact is quantitatively revealed.</p> |
| <b>Suggested Reviewers:</b>                          | Abdelali Oudriss, PhD<br>Professor, Universite de La Rochelle IUT de La Rochelle<br>abdelali.oudriss@univ-lr.fr<br>Professor Oudriss has been working on hydrogen embrittlement for more than ten years with a very comprehensive understanding of this topic. In the past year, he has published many papers focusing on the micro-scaled hydrogen effect on Ni-based   |

|                                |  |
|--------------------------------|--|
|                                | <p>alloys and martensite steels. Professor Oudriss is also an expert in electron microscopy and hydrogen solubility measurement. Therefore, Professor Oudriss is a very qualified reviewer for this paper.</p>   |
|                                | <p>Haiyang Yu, PhD<br/> Oxford University: University of Oxford<br/> haiyang.yu@materials.ox.ac.uk<br/> Dr. Yu has been working on the Discrete Dislocation Dynamics Simulations for many years with very deep understanding on the interaction between dislocations with hydrogen.</p>  |
|                                | <p>Lei Zhang<br/> USTB: University of Science and Technology Beijing<br/> zhanglei@ustb.edu.cn<br/> Professor Zhang has a very rich reasearch experience on the topic of hydrogen embrittlement. He has published many articles about hydrogen effect on metallic alloys with novel analysing methods.</p>   |
|                                | <p>Hisao Matsunaga, PhD<br/> Professor, Kyushu University Faculty of Engineering Graduate School of Engineering:<br/> Kyushu Daigaku Kogakubu Daigakuin Kogakufu<br/> matsunaga.hisao.964@m.kyushu-u.ac.jp<br/> Professor Matsunaga has a very rich reasearch experience on the topic of hydrogen embrittlement. He has published many articles about hydrogen effect on high strength alloys by using in-situ hydrogen charging with nano-scaled novel analysing methods.</p> |
|                                | <p>Milos Djukic, PhD<br/> Professor, University of Belgrade: Univerzitet u Beogradu<br/> mdjukic@mas.bg.ac.rs<br/> Professor Djukic has been working on the hydrogen embrittlement for decades with very deep understanding on the hydrogen effect on material mechanical properties. He has published many journal articles on the topic of hydrogen affected mechanical properties.</p>  |
|                                | <p>Degang Xie, PhD<br/> Professor, Xian Jiaotong University: Xi'an Jiaotong University<br/> dg_xie@xjtu.edu.cn<br/> Professor Xie has rich research experience on nano-scaled in-situ tests with hydrogen charging. In the recent years, he has published several top-level articles in this field, which makes him a very qualified reviewer of this paper.</p>   |
| <b>Opposed Reviewers:</b>      |  |
| <b>Response to Reviewers:</b>  |  |
| <b>Additional Information:</b> |  |
| <b>Question</b>                | <b>Response</b>  |

## Understanding the hydrogen effect on pop-in behavior of an equiatomic high-entropy alloy during in-situ nanoindentation

Dong Wang <sup>a</sup>, Xu Lu <sup>a\*</sup>, Meichao Lin <sup>b</sup>, Di Wan <sup>a</sup>, Zhiming Li <sup>c,d</sup>, Jianying He <sup>b</sup>, Roy Johnsen <sup>a</sup>

<sup>a</sup> Department of Mechanical and Industrial Engineering, Norwegian University of Science and Technology (NTNU), 7491 Trondheim, Norway

<sup>b</sup> Department of Structural Engineering, Norwegian University of Science and Technology (NTNU), 7491 Trondheim, Norway

<sup>c</sup> School of Materials Science and Engineering, Central South University, Changsha, 410083, China

<sup>d</sup> Max-Planck-Institut für Eisenforschung, Max-Planck-Str. 1, 40237 Düsseldorf, Germany

\* Corresponding author: Xu Lu, Email: [xu.lu@ntnu.no](mailto:xu.lu@ntnu.no)

### Abstract

The variations in the pop-in behavior of an equiatomic CoCrFeMnNi high-entropy alloy under different hydrogen charging/discharging conditions were characterized via in-situ electrochemical nanoindentation. Results show that hydrogen accumulatively reduces both pop-in load and width, among which the reduction of pop-in width is more noticeable than that of pop-in load. Moreover, the hydrogen reduction effect on both pop-in load and width is reversible when hydrogen is degassed during anodic discharging process. Particularly, the hydrogen-reduced pop-in width was studied in detail by a comprehensive energy balance model. It is quantitatively shown that the dissolved hydrogen enhances lattice friction, leading to an increased resistance to dislocation motion. As a result, fewer dislocations can be generated with a higher hydrogen concentration, causing a smaller pop-in width. This is the first time that the pop-in width indicated dislocation mobility under hydrogen impact is quantitatively revealed.

Keywords: Nanoindentation; Pop-in; Hydrogen; Dislocation; High-entropy alloy

Hydrogen embrittlement has been recognized as a serious problem in the application of metallic structural materials, where hydrogen degrades the mechanical properties of the material, leading to an unpredictable failure [1-6]. Despite intense studies, the fundamental mechanism of hydrogen embrittlement is still inadequately understood. Recently, it has been widely observed and accepted that the interaction between hydrogen and dislocations is a key factor for causing the embrittlement phenomenon [7-12]. The hydrogen effect on dislocation behavior has been studied by in-situ transmission electron microscopy (TEM), which shows that hydrogen facilitates dislocation motion and promotes planar slip owing to its shielding effect at local stress field [13]. However, the electron beam

produces local heating and high hydrogen fugacity on the thin foil, making this observation difficult to interpret. On the other hand, atomistic simulation has been performed to investigate the hydrogen effect on dislocation mobility, and in contrast, the outcome indicates a resistance to edge dislocation motion by dissolved hydrogen without shielding effect [14].

Nanoindentation is capable of explaining dislocation action by investigating the pop-in behavior, where a sudden displacement burst appears in the load-displacement curve, indicating the transition from elastic to plastic deformation [15, 16]. On a defect-free volume with low dislocation density, the pop-in is usually caused by homogeneous dislocation nucleation [17]. Recently, nanoindentation has been integrated with in-situ electrochemical hydrogen charging (ECNI) to determine the hydrogen effect on dislocation behavior by focusing on the changes of pop-ins under different hydrogen conditions [18-20]. It has been observed that hydrogen can reduce both pop-in load and width of materials with either FCC structure [21-23] or BCC structure [20, 24] under ECNI tests. The hydrogen-reduced pop-in load has been well analyzed and correlated to the hydrogen-enhanced homogeneous dislocation nucleation through the reduction of dislocation line energy and stacking fault energy [21]. However, the mechanism for hydrogen-reduced pop-in width has not been clarified. Therefore, this paper focuses on understanding the hydrogen effect on pop-in width via interpreting the interactions between hydrogen and dislocations.

In the present study, an equiatomic high-entropy alloy (HEA) with nominal composition  $\text{Co}_{20}\text{Cr}_{20}\text{Fe}_{20}\text{Mn}_{20}\text{Ni}_{20}$  (at. %) was used. It was cast, hot rolled, and homogenized at 1200 °C for 2 h followed by water quenching. The samples used for ECNI test were further machined into discs with a diameter of 11.8 mm and a thickness of 2 mm. The surfaces were prepared by mechanical grinding and polishing till 1  $\mu\text{m}$  diamond paste, followed by electropolishing in a methanol/ $\text{H}_2\text{SO}_4$  solution at 25 V for 60 s to ensure a non-deformed surface. The ECNI test was performed by using Hysitron Triboindenter TI 950 equipped with a specially designed long-shaft Berkovich diamond tip. An electrochemical cell consisting of a platinum counter electrode and a  $\text{Hg}/\text{HgSO}_4$  reference electrode was used for in-situ hydrogen charging. The electrolyte consisted of glycerol-based borax (with 0.002 mol/L  $\text{Na}_2\text{S}_2\text{O}_3$ ) that is reliable for ECNI test by keeping the sample surface from corrosion due to its extremely low solubility and diffusivity of oxygen [25, 26]. More details about the electrochemical charging can be found in Ref. [21]. The testing was firstly performed in air condition, followed by a sequence of cathodic charging at -1300 (H1), -1400 (H2), and -1500 mV (H3) vs.  $\text{Hg}/\text{HgSO}_4$ . After the cathodic charging process, an anodic discharging at 0 mV was performed to check the reversibility of the hydrogen effect. Each charging and discharging process was applied for 2 h to ensure enough hydrogen absorbed and desorbed in the surface area. To eliminate the influence of different grain orientations, all the tests were performed in an (111)-direction grain (The detailed experimental procedures are shown in the supplementary document). The load function consists of a linear loading segment (8000  $\mu\text{N}/\text{s}$ ) till 2000  $\mu\text{N}$  with a holding time of 0.45 s, followed by a linear unloading segment

until 10% of the peak value with an additional 0.25 s holding segment for drift correction. At least 18 indentations were performed in each condition to guarantee the reproducibility.

Figure 1 shows the load-displacement curves under each charging/discharging condition. Specifically, Figure 1a presents the curves obtained in air condition before hydrogen charging; Figures 1b-1d show the curves during hydrogen charging with an increasing charging potential from H1 (-1300 mV) to H3 (-1500 mV). The corresponding surface hydrogen concentrations were calculated to be 11.76, 25.67, and 31.43 wppm, respectively (detailed calculations are shown in the supplementary document); Curves in Figure 1e were attained during the following anodic discharging process, where the dissolved hydrogen was diffused out of the sample surface. All the load-displacement curves present a clear pop-in phenomenon that can be linked to the homogeneous dislocation nucleation beneath the indenter, where the maximum shear stress exceeds the theoretical critical shear stress for dislocation nucleation [16, 27]. It has also been reported that the pop-ins might relate to the heterogeneous dislocation nucleation, where the pre-existed dislocations were activated during nanoindentation [28]. However, this is not the case for the current study, because the dislocation density in the annealed sample was very low with a mean dislocation spacing of 0.5-0.8  $\mu\text{m}$ , which was confirmed by the previous studies [22, 29]. Moreover, the material exhibits a relatively “clean microstructure” without too many pre-existing defects [22]. During nanoindentation, the pop-in occurs at a depth of around 15 nm, which results in a stressed volume with a size that is much smaller than the mean dislocation spacing [30-35]. Therefore, an indent placed randomly on sample surface has a high probability of probing on an area without pre-existed dislocations, and therefore the pop-ins in the current study indicate the homogeneous nucleation of dislocations.

Figure 1f presents the mean values of pop-in load  $p$  and width  $\Delta h$  under each condition. It clearly shows that the introduction of hydrogen results in both reduced  $p$  and  $\Delta h$ . This reduction effect became more pronounced with a higher surface hydrogen concentration when increasing the charging potential from H1 to H3. Moreover, during anodic discharging process, where the dissolved hydrogen was degassed, both  $p$  and  $\Delta h$  recovered to their original values as in air condition. The recovered pop-in behavior in anodic condition, together with the constant surface quality (Figure 1a and 1e), can be used to exclude the impact of surface roughness on pop-in behavior. Therefore, the only influencing factor in this study is the different amount of dissolved hydrogen. Moreover, despite the fact that hydrogen reduces both  $p$  and  $\Delta h$ , it is noticeable that the reduction of  $\Delta h$  is much more pronounced than the reduction of  $p$  value. This phenomenon can be better observed by plotting each  $p$  value against the corresponding  $\Delta h$  value, as shown in Figure 2. An approximately linear relation between  $p$  and  $\Delta h$  can be observed in each testing condition, which is in consistence with former studies [28, 36]. These linear relations show an increased slope with an increasing amount of charged hydrogen, indicating a major hydrogen effect on  $\Delta h$ . The dashed line in Figure 2 shows an example when the pop-ins happened at a similar load (400  $\mu\text{N}$ ), the  $\Delta h$  value is reduced from 32 nm in air condition down to 26, 18, and 14 nm under the hydrogen charging

conditions from H1 to H3, respectively. The hydrogen reduced  $\Delta h$  has been reported in several studies [17, 21], but the intrinsic reason remains unexplored. To illustrate the fundamental mechanism, we present a model which is based on the energy equilibrium of the subsurface system during nanoindentation test, as discussed below.

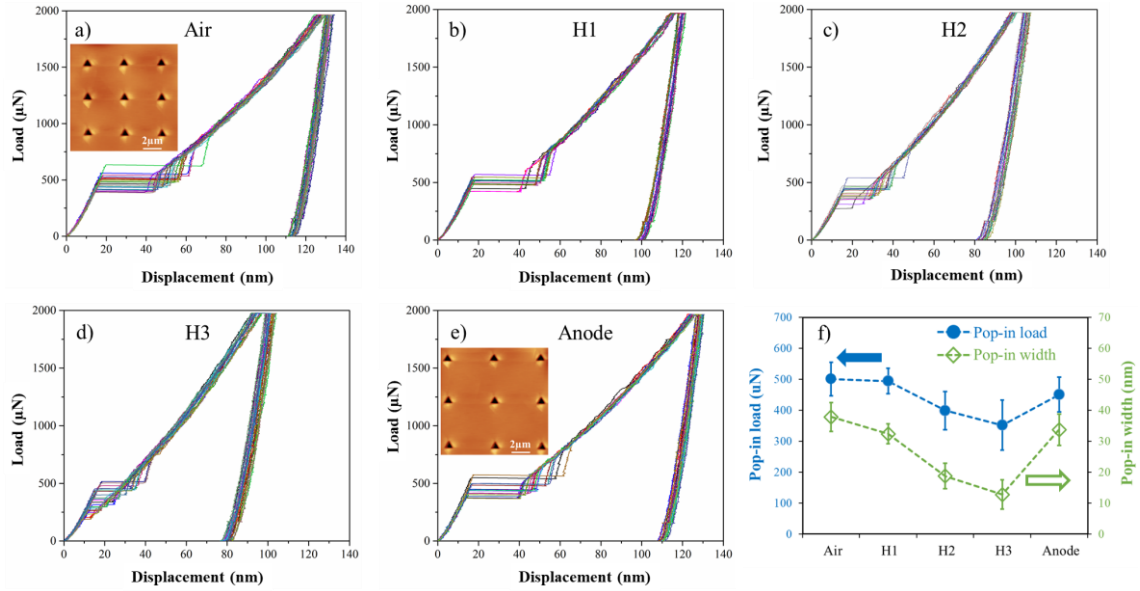


Figure 1: Load-displacement curves in (a) air, under the hydrogen charging conditions at (b) H1 (-1300 mV), (c) H2 (-1400 mV), (d) H3 (-1500 mV), and (e) anodic hydrogen discharging condition. The surface quality before and after hydrogen charging are shown as the insets in (a) and (e), respectively. (f) shows the pop-in width  $\Delta h$  and pop-in load  $p$  under different hydrogen charging conditions.

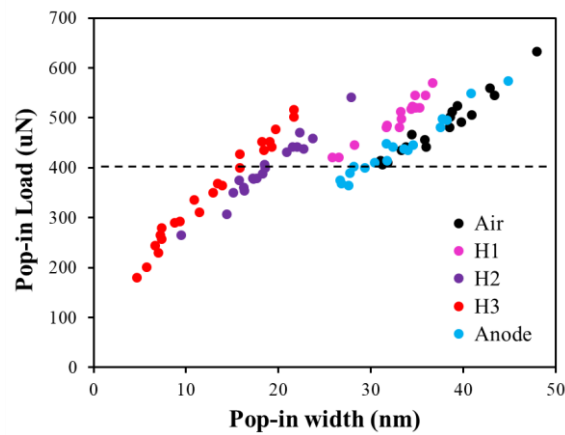


Figure 2: Relation between pop-in width and pop-in load under different hydrogen charging conditions. Dashed line shows an example of the major hydrogen effect on pop-in width.

The energy balance criterion proposes that the total stored elastic energy  $W_e$  before pop-in is dissipated by the plastic work during the pop-in process [37-39]. The value of  $W_e$  is given by the shaded area in Figure 3a, and can be calculated using the equation of

$$W_e = \int_0^{h_1} P(h)dh \quad (1)$$

where  $P$  is the load,  $h$  is the depth during nanoindentation test, and  $h_1$  is the depth where the pop-in begins. The Berkovich tip in this study can be treated as a spherical indenter tip at a very small indent depth until the pop-in happens ( $\sim 15$  nm). Hence, the relation between load and depth during elastic loading can be evaluated using the Hertzian contact theory [27] as:

$$P(h) = \frac{4}{3} E_r h^{3/2} R^{1/2} \quad (2)$$

here,  $E_r$  is the reduced elastic modulus that can be obtained by fitting the elastic segment of the loading curve (Figure 3a) with Eq. (2).  $R$  is the tip radius that equals to  $0.98 \mu\text{m}$  for the current study. Therefore, by integrating Eqs. (1) and (2), the total stored elastic energy during the initial elastic loading can be obtained as:

$$W_e = \int_0^{h_1} P(h)dh = \frac{8}{15} E_r R^{1/2} h_1^{5/2} \quad (3)$$

In the current study, the dislocation configuration beneath the indenter is assumed to be a stack of prismatic dislocation loops with a radius of  $r$  and a distance of  $d$  as shown in Figure 3b [38]. It is also assumed that the Burgers vector is normal to the loop plane and defines the slip steps. These assumptions are made with the support of former molecular dynamics simulations [40, 41]. Therefore, the total stored elastic energy  $W_e$  is proposed to be exhausted by the accumulation of geometrically necessary dislocations emitted from the point beneath the indenter experiencing the maximum shear stress. Based on the overall energy balance,  $W_e$  can be expressed as the summation of the total interaction energy between dislocations  $W_i^t$ , the total dislocation line energy  $W_s$ , and the total friction energy  $W_f^t$  consumed by the movement of dislocations as follows [40]:

$$W_e = W_i^t + N \cdot W_s + W_f^t \quad (4)$$

here,  $N$  is the number of generated dislocation loops, which is suggested to be related to  $\Delta h$ , because the generation of dislocations underneath the tip must accommodate the displacement of the indenter. The relation between the number of dislocation loops and pop-in width has been proposed as  $N = \Delta h / (2b)$  [37].  $b$  is the magnitude of Burgers vector, which was calculated from the lattice parameter ( $a$ ) for the studied material divided by the square-root of two as  $a/2[101]$  and equals to  $0.25 \text{ nm}$  [42-45].

The interaction energy between two circular prismatic dislocation loops can be expressed as [46]:

$$W_i = \frac{\mu b^2}{1-\nu} r \left( \ln \frac{8r}{d} - 1 \right) \quad (5)$$

where  $\mu$  is the shear modulus that can be determined from Poisson's ratio ( $\nu = 0.27$ ) and elastic modulus. The distance between dislocation loops  $d$  is set equal to  $b$ , if we assume the prismatic dislocation loops are continuously emitted and close-packed (Figure 3b) [38]. The radius of dislocation loops  $r$  can be estimated from the distribution of shear stress underneath the indenter shown in Figure 3c. The graphical representation of the maximum shear stress with the axis normalized to the contact radius ( $a_c = \sqrt[3]{\frac{3PR}{4E_r}}$ ) is constructed based on the Hertz-Huber model [47]. It shows that the highest value of maximum shear stress happens at the point  $0.48a_c$  below the indenter [48]. Since the maximum shear stress happens at a point, it is reasonable to estimate a region, where 98% of the maximum shear stress is acting, as the size of generated dislocation loops [20, 31]. The intersecting plane in Figure 3c defines the 98% of the maximum shear stress, and it results in a semi-elliptical region with a major half-axis of  $0.29 a_c$ , which was chosen as the radius of dislocation loop.

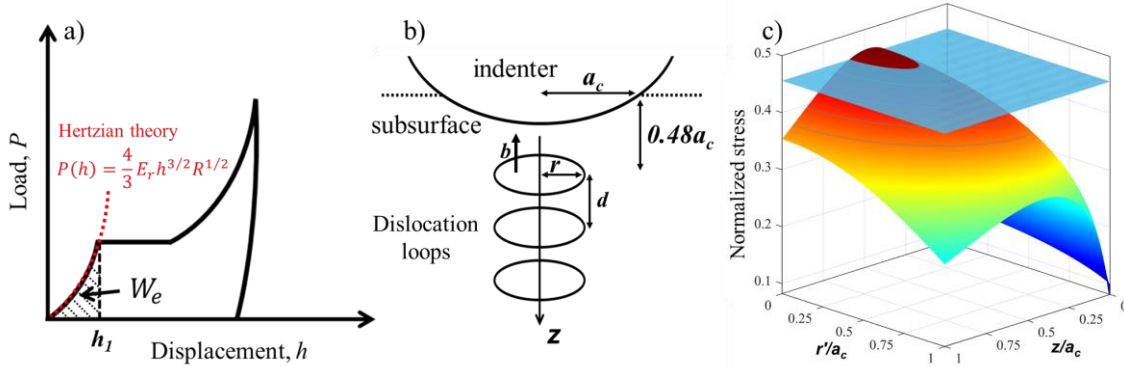


Figure 3: a) Stored elastic energy for dislocation nucleation. b) The schematic of prismatic dislocation loops beneath the indenter generated during pop-in. c) Distribution of maximum shear stress beneath the indenter according to Hertz-Huber model. The plane defines 98% of the maximum shear stress.

The total dislocation interaction energy  $W_i^t$  can be obtained by the summation over all interactions between each loop with all the rest loops, and it would give rise to the following relation [46]:

$$W_i^t = \frac{\mu b^2}{1-\nu} r \left( \left\{ \sum_{j=1}^{N-1} j \left( \ln \frac{8r}{d} \right) - \sum_{j=1}^{N-1} \ln(j!) - \sum_{j=1}^{N-1} j \right\} \right) \quad (6)$$

Also, the dislocation line energy is expressed as [49]:

$$W_s = \frac{\mu b^2}{2(1-\nu)} r \left( \ln \frac{8r}{\rho} - 1 \right) \quad (7)$$

where  $\rho$  is the radius of dislocation core and it is here equal to  $b/2$  [39]. Thus, the total dislocation line energy of  $N$  circular loops equals to  $N \times W_s$ . Therefore, the values of  $W_e$ ,  $W_i^t$ ,  $N$ , and  $W_s$  in Eq. 4 can be quantitatively calculated from the nanoindentation results. The only unknown part in Eq. 4 is the total friction energy  $W_f^t$  for dislocation motion. All the dislocation loops are assumed to be emitted from the same area beneath the indenter, followed by slipping along the indenting direction, and close-pack with a Burgers vector distance as shown in Figure 3b. Due to this, the unit friction energy  $W_f$ , as the energy for a dislocation loop to move  $b$  distance, can be expressed as  $W_f \cdot \frac{N(N-1)}{2} = W_f^t$ . The item  $N(N-1)/2$  indicates the total number of slip steps for generating  $N$  prismatic dislocation loops. By integrating Eqs. 3-7, the unit friction energy for dislocation slip in each charging condition during pop-in phenomenon can be calculated. **The cumulative frequency distribution analysis [50] on unit friction energy in different conditions is shown in Figure 4.** It shows that the average unit friction energy in air condition without hydrogen charging was  $1.86 \times 10^{-16}$  J, which increased to  $6.44 \times 10^{-16}$ ,  $2.79 \times 10^{-15}$ ,  $7.55 \times 10^{-15}$  J with 2.5, 14.0, and 39.6 times increment during hydrogen charging at H1, H2, and H3, respectively. When anodic discharging was applied, the average unit friction energy returned to  $2.56 \times 10^{-16}$  J, which is only 0.37 times higher than the value in air condition. The trapped hydrogen that cannot diffuse out during anodic discharging process might results in this minor remained increment.

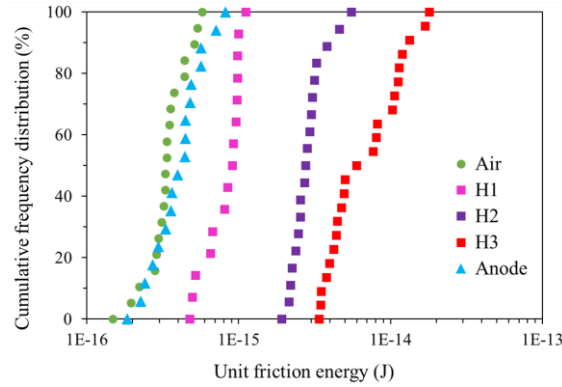


Figure 4: The cumulative frequency distribution of unit friction energy for dislocation motion at the instant of pop-in.

A very clear hydrogen-enhanced friction for dislocation motion can be concluded from Figure 4. During the pop-in process, the shear stress beneath the indenter will nucleate and drive dislocations. When hydrogen charging is applied, the hydrogen atoms are absorbed and dissolved into the subsurface of the material. On the one hand, the dissolved hydrogen enhances homogeneous dislocation nucleation through the reduction of dislocation line energy, as proposed by the former studies [21, 24], resulting in a reduced pop-in load. On the other hand, these hydrogen atoms are accumulated forming Cottrell-

like atmosphere around moving dislocations and perform substantial resistance to dislocation motion, which is consistent with the solute drag theory [14, 49, 51]. Thus, each dislocation slip step needs more energy to overcome the enhanced friction. As a result, substantial stored elastic energy will be consumed by the hydrogen-induced lattice friction and it ends up with a fewer amount of generated dislocations and a smaller pop-in width. In brief, hydrogen enhances dislocation nucleation, while impedes dislocation motion. When a higher hydrogen concentration is applied, it will enhance the induced friction, and the pop-in width is further reduced. This hydrogen-resisted dislocation motion has also been revealed by other researchers from both atomistic simulations [14, 52] and in-situ experimental studies [9, 39]. While under the anodic discharging, the dissolved hydrogen is mostly diffused out of the sample surface, and both hydrogen-induced lattice friction and hydrogen Cottrell atmosphere are eliminated. Therefore, the pop-in width is recovered to its original value in air. However, it shows that the unit friction energy in anodic condition is still slightly higher (by 0.37 times) than in air. This minor increment might be due to the relatively low amount of deep trapped hydrogen, which cannot diffuse out during anodic discharging.

In summary, the influence of hydrogen on the pop-in behavior was investigated in an equiatomic CoCrFeMnNi HEA through in-situ electrochemical nanoindentation test. The results show that hydrogen accumulatively affects the relation between pop-in width and load, where the reduction effect is more noticeable for width than load. By analyzing the interactions between hydrogen and dislocations via a comprehensive energy balance model, it was quantitatively interpreted as the enhanced lattice friction by hydrogen in consistent with the solute drag theory. As a result, fewer dislocations can be generated with a smaller pop-in width under the hydrogen charging condition. This is the first time that the intrinsic relation between hydrogen and dislocation motion related pop-in width has been quantitatively revealed, which provides unambiguous insights in the hydrogen-interrelated failure mechanisms.

## **Acknowledgements**

The authors are grateful for the support provided by Research Council of Norway through the HyLINE (294739) and M-HEAT (294689) projects. Z.L. would like to acknowledge the financial support by the Hunan Special Funding for the Construction of Innovative Province (2019RS1001).

## **Data availability**

The data that support the findings of this study are available on request from the corresponding author. The data are not publicly available as the data also forms part of an ongoing study.

## Reference:

- [1] S. Lynch, *Corros. Rev.* 30(3-4) (2012) 105-123.
- [2] A. Oudriss, J. Creus, J. Bouhattate, E. Conforto, C. Berziou, C. Savall, X. Feaugas, *Acta Mater.* 60(19) (2012) 6814-6828.
- [3] M.B. Djukic, V. Sijacki Zeravcic, G.M. Bakic, A. Sedmak, B. Rajcic, *Engineering Failure Analysis* 58 (2015) 485-498.
- [4] B. Sun, D. Wang, X. Lu, D. Wan, D. Ponge, X. Zhang, *Acta Metallurgica Sinica (English Letters)* (2021).
- [5] D. Wang, X. Lu, D. Wan, X. Guo, R. Johnsen, *Mater. Sci. Eng. A* (2020) 140638.
- [6] D. Wan, Y. Ma, B. Sun, S.M.J. Razavi, D. Wang, X. Lu, W. Song, *Journal of Materials Science & Technology* 85 (2021) 30-43.
- [7] H. Yu, A. Cocks, E. Tarleton, *J. Mech. Phys. Solids* (2018).
- [8] I.M. Robertson, P. Sofronis, A. Nagao, M.L. Martin, S. Wang, D.W. Gross, K.E. Nygren, *Metall. Mater. Trans. A* 46a(6) (2015) 2323-2341.
- [9] D.G. Xie, S.Z. Li, M. Li, Z.J. Wang, P. Gumbsch, J. Sun, E. Ma, J. Li, Z.W. Shan, *Nat. Commun.* 7 (2016).
- [10] X. Lu, D. Wang, D. Wan, Z.B. Zhang, N. Kheradmand, A. Barnoush, *Acta Mater.* 179 (2019) 36-48.
- [11] R. Kirchheim, *Scr. Mater.* 62(2) (2010) 67-70.
- [12] X. Lu, Y. Ma, D. Wang, *Mater. Sci. Eng. A* 792 (2020) 139785.
- [13] P. Ferreira, I. Robertson, H. Birnbaum, *Acta Mater.* 46(5) (1998) 1749-1757.
- [14] J. Song, W.A. Curtin, *Acta Mater.* 68 (2014) 61-69.
- [15] M.-Y. Seok, I.-C. Choi, J. Moon, S. Kim, U. Ramamurty, J.-i. Jang, *Scr. Mater.* 87 (2014) 49-52.
- [16] S. Shim, H. Bei, E.P. George, G.M. Pharr, *Scr. Mater.* 59(10) (2008) 1095-1098.
- [17] A. Barnoush, M.T. Welsch, H. Vehoff, *Scr. Mater.* 63(5) (2010) 465-468.
- [18] G. Hachet, A. Oudriss, A. Barnoush, T. Hajilou, D. Wang, A. Metsue, X. Feaugas, *Mater. Sci. Eng. A* (2020) 140480.
- [19] D. Wang, X. Lu, D. Wan, Z. Li, A. Barnoush, *Scr. Mater.* 173 (2019) 56-60.
- [20] A. Barnoush, H. Vehoff, *Acta Mater.* 58(16) (2010) 5274-5285.
- [21] D. Wang, X. Lu, Y. Deng, X. Guo, A. Barnoush, *Acta Mater.* 166 (2019) 618-629.
- [22] D. Wang, X. Lu, Y. Deng, D. Wan, Z. Li, A. Barnoush, *Intermetallics* 114 (2019) 106605.
- [23] G. Stenerud, R. Johnsen, J.S. Olsen, J.Y. He, A. Barnoush, *Int. J. Hydrog. Energy* 42(24) (2017) 15933-15942.
- [24] A. Bamoush, N. Kheradmand, T. Hajilou, *Scr. Mater.* 108 (2015) 76-79.
- [25] X. Lu, D. Wang, *Journal of Materials Science & Technology* 67 (2021) 243-253.
- [26] X. Lu, D. Wang, Z. Li, Y. Deng, A. Barnoush, *Mater. Sci. Eng. A* 762 (2019) 138114.
- [27] K.L. Johnson, *Contact Mechanics*, Cambridge University Press, Cambridge, 1987.
- [28] F. Pöhl, *Sci. Rep.* 9(1) (2019).
- [29] I. Gutierrez-Urrutia, S. Zaeferrer, D. Raabe, *Scr. Mater.* 61(7) (2009) 737-740.
- [30] Y. Zhao, J.-M. Park, J.-i. Jang, U. Ramamurty, *Acta Mater.* 202 (2021) 124-134.
- [31] A. Barnoush, *Acta Mater.* 60(3) (2012) 1268-1277.
- [32] H. Bei, Z.P. Lu, E.P. George, *Phys. Rev. Lett.* 93(12) (2004).
- [33] J.R. Morris, H. Bei, G.M. Pharr, E.P. George, *Phys. Rev. Lett.* 106(16) (2011) 165502.
- [34] D. Wu, J.R. Morris, T.G. Nieh, *Scr. Mater.* 94 (2015) 52-55.
- [35] K. Gan, D. Yan, S. Zhu, Z. Li, *Acta Mater.* 206 (2021) 116633.
- [36] C. Müller, M. Zamanzade, C. Motz, *Micromachines* 10(2) (2019) 114.
- [37] C. Shin, S. Shim, *J. Mater. Res.* 27(16) (2012) 2161-2166.
- [38] A. Gouldstone, H.J. Koh, K.Y. Zeng, A.E. Giannakopoulos, S. Suresh, *Acta Mater.* 48(9) (2000) 2277-2295.
- [39] A. Barnoush, M. Asgari, R. Johnsen, *Scr. Mater.* 66(6) (2012) 414-417.
- [40] Y. Shibutani, T. Tsuru, A. Koyama, *Acta Mater.* 55(5) (2007) 1813-1822.
- [41] K. Zhao, J. He, A.E. Mayer, Z. Zhang, *Acta Mater.* 148 (2018) 18-27.
- [42] A. Heczal, M. Kawasaki, J.L. Lábár, J.-i. Jang, T.G. Langdon, J. Gubicza, *J. Alloys Compd.* 711 (2017) 143-154.

- [43] L.R. Owen, E.J. Pickering, H.Y. Playford, H.J. Stone, M.G. Tucker, N.G. Jones, *Acta Mater.* 122 (2017) 11-18.
- [44] B. Cantor, I.T.H. Chang, P. Knight, A.J.B. Vincent, *Mater. Sci. Eng. A* 375-377 (2004) 213-218.
- [45] J.Y. He, H. Wang, H.L. Huang, X.D. Xu, M.W. Chen, Y. Wu, X.J. Liu, T.G. Nieh, K. An, Z.P. Lu, *Acta Mater.* 102 (2016) 187-196.
- [46] P.M. Anderson, J.P. Hirth, J. Lothe, *Theory of Dislocations*, 3rd ed., Cambridge University Press, Cambridge, 2017.
- [47] M.T. Huber, *Annalen der Physik* 319(6) (1904) 153-163.
- [48] W.D. Nix, H.J. Gao, *J. Mech. Phys. Solids* 46(3) (1998) 411-425.
- [49] D. Hull, D.J. Bacon, *Introduction to Dislocations*, Elsevier Science 2011.
- [50] H.P. Ritzema, *Drainage principles and applications*; 3rd ed, ILRI, Wageningen, 2006.
- [51] A.H. Cottrell, *Dislocations and plastic flow in crystals*, Clarendon Press, Oxford, 1953.
- [52] Y. Zhu, Z. Li, M. Huang, H. Fan, *Int. J. Plast.* 92 (2017) 31-44.

# Understanding the hydrogen effect on pop-in behavior of an equiatomic high-entropy alloy during in-situ nanoindentation

Dong Wang <sup>a</sup>, Xu Lu <sup>a\*</sup>, Meichao Lin <sup>b</sup>, Di Wan <sup>a</sup>, Zhiming Li <sup>c,d</sup>, Jianying He <sup>b</sup>, Roy Johnsen <sup>a</sup>

<sup>a</sup> Department of Mechanical and Industrial Engineering, Norwegian University of Science and Technology (NTNU), 7491 Trondheim, Norway

<sup>b</sup> Department of Structural Engineering, Norwegian University of Science and Technology (NTNU), 7491 Trondheim, Norway

<sup>c</sup> School of Materials Science and Engineering, Central South University, Changsha, 410083, China

<sup>d</sup> Max-Planck-Institut für Eisenforschung, Max-Planck-Str. 1, 40237 Düsseldorf, Germany

\* Corresponding author: Xu Lu, Email: [xu.lu@ntnu.no](mailto:xu.lu@ntnu.no)

## Abstract

The variations in the pop-in behavior of an equiatomic CoCrFeMnNi high-entropy alloy under different hydrogen charging/discharging conditions were characterized via in-situ electrochemical nanoindentation. Results show that hydrogen accumulatively reduces both pop-in load and width, among which the reduction of pop-in width is more noticeable than that of pop-in load. Moreover, the hydrogen reduction effect on both pop-in load and width is reversible when hydrogen is degassed during anodic discharging process. Particularly, the hydrogen-reduced pop-in width was studied in detail by a comprehensive energy balance model. It is quantitatively shown that the dissolved hydrogen enhances lattice friction, leading to an increased resistance to dislocation motion. As a result, fewer dislocations can be generated with a higher hydrogen concentration, causing a smaller pop-in width. This is the first time that the pop-in width indicated dislocation mobility under hydrogen impact is quantitatively revealed.

Keywords: Nanoindentation; Pop-in; Hydrogen; Dislocation; High-entropy alloy

Hydrogen embrittlement has been recognized as a serious problem in the application of metallic structural materials, where hydrogen degrades the mechanical properties of the material, leading to an unpredictable failure [1-6]. Despite intense studies, the fundamental mechanism of hydrogen embrittlement is still inadequately understood. Recently, it has been widely observed and accepted that the interaction between hydrogen and dislocations is a key factor for causing the embrittlement phenomenon [7-12]. The hydrogen effect on dislocation behavior has been studied by in-situ transmission electron microscopy (TEM), which shows that hydrogen facilitates dislocation motion and promotes planar slip owing to its shielding effect at local stress field [13]. However, the electron beam

produces local heating and high hydrogen fugacity on the thin foil, making this observation difficult to interpret. On the other hand, atomistic simulation has been performed to investigate the hydrogen effect on dislocation mobility, and in contrast, the outcome indicates a resistance to edge dislocation motion by dissolved hydrogen without shielding effect [14].

Nanoindentation is capable of explaining dislocation action by investigating the pop-in behavior, where a sudden displacement burst appears in the load-displacement curve, indicating the transition from elastic to plastic deformation [15, 16]. On a defect-free volume with low dislocation density, the pop-in is usually caused by homogeneous dislocation nucleation [17]. Recently, nanoindentation has been integrated with in-situ electrochemical hydrogen charging (ECNI) to determine the hydrogen effect on dislocation behavior by focusing on the changes of pop-ins under different hydrogen conditions [18-20]. It has been observed that hydrogen can reduce both pop-in load and width of materials with either FCC structure [21-23] or BCC structure [20, 24] under ECNI tests. The hydrogen-reduced pop-in load has been well analyzed and correlated to the hydrogen-enhanced homogeneous dislocation nucleation through the reduction of dislocation line energy and stacking fault energy [21]. However, the mechanism for hydrogen-reduced pop-in width has not been clarified. Therefore, this paper focuses on understanding the hydrogen effect on pop-in width via interpreting the interactions between hydrogen and dislocations.

In the present study, an equiatomic high-entropy alloy (HEA) with nominal composition  $\text{Co}_{20}\text{Cr}_{20}\text{Fe}_{20}\text{Mn}_{20}\text{Ni}_{20}$  (at. %) was used. It was cast, hot rolled, and homogenized at 1200 °C for 2 h followed by water quenching. The samples used for ECNI test were further machined into discs with a diameter of 11.8 mm and a thickness of 2 mm. The surfaces were prepared by mechanical grinding and polishing till 1  $\mu\text{m}$  diamond paste, followed by electropolishing in a methanol/ $\text{H}_2\text{SO}_4$  solution at 25 V for 60 s to ensure a non-deformed surface. The ECNI test was performed by using Hysitron Triboindenter TI 950 equipped with a specially designed long-shaft Berkovich diamond tip. An electrochemical cell consisting of a platinum counter electrode and a  $\text{Hg}/\text{HgSO}_4$  reference electrode was used for in-situ hydrogen charging. The electrolyte consisted of glycerol-based borax (with 0.002 mol/L  $\text{Na}_2\text{S}_2\text{O}_3$ ) that is reliable for ECNI test by keeping the sample surface from corrosion due to its extremely low solubility and diffusivity of oxygen [25, 26]. More details about the electrochemical charging can be found in Ref. [21]. The testing was firstly performed in air condition, followed by a sequence of cathodic charging at -1300 (H1), -1400 (H2), and -1500 mV (H3) vs.  $\text{Hg}/\text{HgSO}_4$ . After the cathodic charging process, an anodic discharging at 0 mV was performed to check the reversibility of the hydrogen effect. Each charging and discharging process was applied for 2 h to ensure enough hydrogen absorbed and desorbed in the surface area. To eliminate the influence of different grain orientations, all the tests were performed in an (111)-direction grain (The detailed experimental procedures are shown in the supplementary document). The load function consists of a linear loading segment (8000  $\mu\text{N}/\text{s}$ ) till 2000  $\mu\text{N}$  with a holding time of 0.45 s, followed by a linear unloading segment

until 10% of the peak value with an additional 0.25 s holding segment for drift correction. At least 18 indentations were performed in each condition to guarantee the reproducibility.

Figure 1 shows the load-displacement curves under each charging/discharging condition. Specifically, Figure 1a presents the curves obtained in air condition before hydrogen charging; Figures 1b-1d show the curves during hydrogen charging with an increasing charging potential from H1 (-1300 mV) to H3 (-1500 mV). The corresponding surface hydrogen concentrations were calculated to be 11.76, 25.67, and 31.43 wppm, respectively (detailed calculations are shown in the supplementary document); Curves in Figure 1e were attained during the following anodic discharging process, where the dissolved hydrogen was diffused out of the sample surface. All the load-displacement curves present a clear pop-in phenomenon that can be linked to the homogeneous dislocation nucleation beneath the indenter, where the maximum shear stress exceeds the theoretical critical shear stress for dislocation nucleation [16, 27]. It has also been reported that the pop-ins might relate to the heterogeneous dislocation nucleation, where the pre-existed dislocations were activated during nanoindentation [28]. However, this is not the case for the current study, because the dislocation density in the annealed sample was very low with a mean dislocation spacing of 0.5-0.8  $\mu\text{m}$ , which was confirmed by the previous studies [22, 29]. Moreover, the material exhibits a relatively “clean microstructure” without too many pre-existing defects [22]. During nanoindentation, the pop-in occurs at a depth of around 15 nm, which results in a stressed volume with a size that is much smaller than the mean dislocation spacing [30-35]. Therefore, an indent placed randomly on sample surface has a high probability of probing on an area without pre-existed dislocations, and therefore the pop-ins in the current study indicate the homogeneous nucleation of dislocations.

Figure 1f presents the mean values of pop-in load  $p$  and width  $\Delta h$  under each condition. It clearly shows that the introduction of hydrogen results in both reduced  $p$  and  $\Delta h$ . This reduction effect became more pronounced with a higher surface hydrogen concentration when increasing the charging potential from H1 to H3. Moreover, during anodic discharging process, where the dissolved hydrogen was degassed, both  $p$  and  $\Delta h$  recovered to their original values as in air condition. The recovered pop-in behavior in anodic condition, together with the constant surface quality (Figure 1a and 1e), can be used to exclude the impact of surface roughness on pop-in behavior. Therefore, the only influencing factor in this study is the different amount of dissolved hydrogen. Moreover, despite the fact that hydrogen reduces both  $p$  and  $\Delta h$ , it is noticeable that the reduction of  $\Delta h$  is much more pronounced than the reduction of  $p$  value. This phenomenon can be better observed by plotting each  $p$  value against the corresponding  $\Delta h$  value, as shown in Figure 2. An approximately linear relation between  $p$  and  $\Delta h$  can be observed in each testing condition, which is in consistence with former studies [28, 36]. These linear relations show an increased slope with an increasing amount of charged hydrogen, indicating a major hydrogen effect on  $\Delta h$ . The dashed line in Figure 2 shows an example when the pop-ins happened at a similar load (400  $\mu\text{N}$ ), the  $\Delta h$  value is reduced from 32 nm in air condition down to 26, 18, and 14 nm under the hydrogen charging

conditions from H1 to H3, respectively. The hydrogen reduced  $\Delta h$  has been reported in several studies [17, 21], but the intrinsic reason remains unexplored. To illustrate the fundamental mechanism, we present a model which is based on the energy equilibrium of the subsurface system during nanoindentation test, as discussed below.

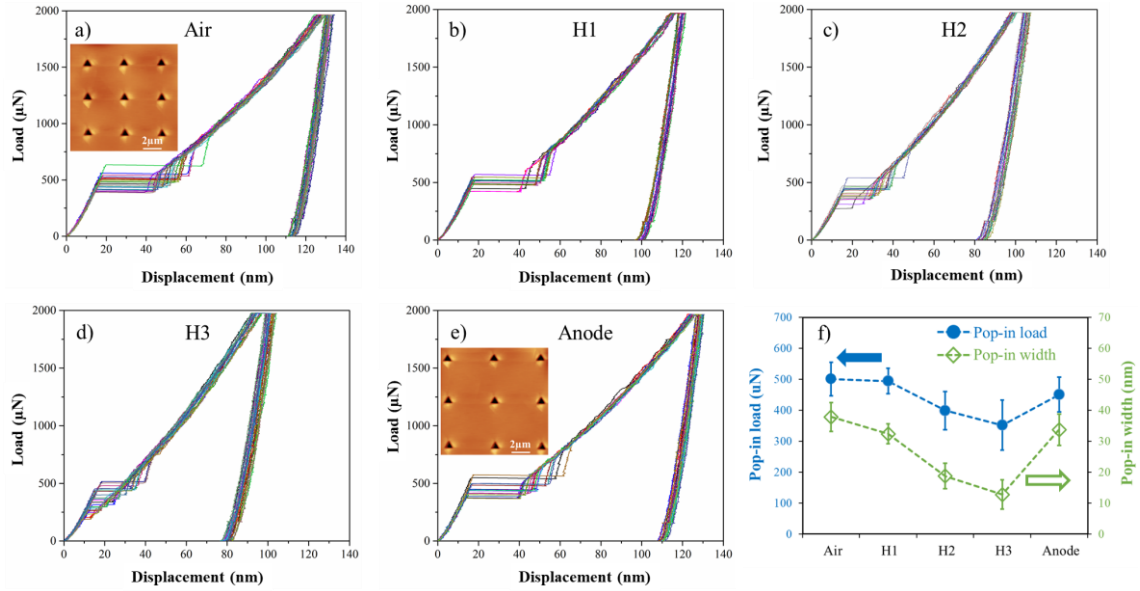


Figure 1: Load-displacement curves in (a) air, under the hydrogen charging conditions at (b) H1 (-1300 mV), (c) H2 (-1400 mV), (d) H3 (-1500 mV), and (e) anodic hydrogen discharging condition. The surface quality before and after hydrogen charging are shown as the insets in (a) and (e), respectively. (f) shows the pop-in width  $\Delta h$  and pop-in load  $p$  under different hydrogen charging conditions.

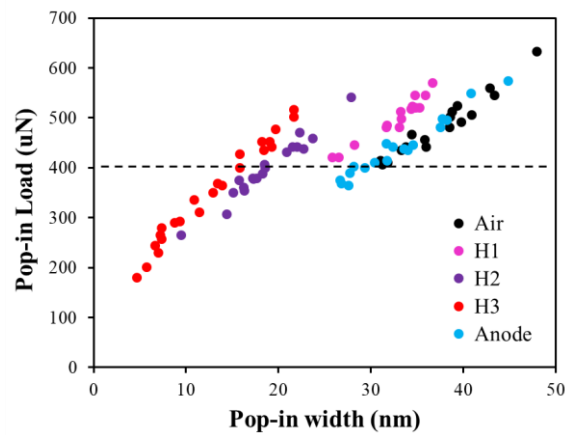


Figure 2: Relation between pop-in width and pop-in load under different hydrogen charging conditions. Dashed line shows an example of the major hydrogen effect on pop-in width.

The energy balance criterion proposes that the total stored elastic energy  $W_e$  before pop-in is dissipated by the plastic work during the pop-in process [37-39]. The value of  $W_e$  is given by the shaded area in Figure 3a, and can be calculated using the equation of

$$W_e = \int_0^{h_1} P(h)dh \quad (1)$$

where  $P$  is the load,  $h$  is the depth during nanoindentation test, and  $h_1$  is the depth where the pop-in begins. The Berkovich tip in this study can be treated as a spherical indenter tip at a very small indent depth until the pop-in happens ( $\sim 15$  nm). Hence, the relation between load and depth during elastic loading can be evaluated using the Hertzian contact theory [27] as:

$$P(h) = \frac{4}{3} E_r h^{3/2} R^{1/2} \quad (2)$$

here,  $E_r$  is the reduced elastic modulus that can be obtained by fitting the elastic segment of the loading curve (Figure 3a) with Eq. (2).  $R$  is the tip radius that equals to  $0.98 \mu\text{m}$  for the current study. Therefore, by integrating Eqs. (1) and (2), the total stored elastic energy during the initial elastic loading can be obtained as:

$$W_e = \int_0^{h_1} P(h)dh = \frac{8}{15} E_r R^{1/2} h_1^{5/2} \quad (3)$$

In the current study, the dislocation configuration beneath the indenter is assumed to be a stack of prismatic dislocation loops with a radius of  $r$  and a distance of  $d$  as shown in Figure 3b [38]. It is also assumed that the Burgers vector is normal to the loop plane and defines the slip steps. These assumptions are made with the support of former molecular dynamics simulations [40, 41]. Therefore, the total stored elastic energy  $W_e$  is proposed to be exhausted by the accumulation of geometrically necessary dislocations emitted from the point beneath the indenter experiencing the maximum shear stress. Based on the overall energy balance,  $W_e$  can be expressed as the summation of the total interaction energy between dislocations  $W_i^t$ , the total dislocation line energy  $W_s$ , and the total friction energy  $W_f^t$  consumed by the movement of dislocations as follows [40]:

$$W_e = W_i^t + N \cdot W_s + W_f^t \quad (4)$$

here,  $N$  is the number of generated dislocation loops, which is suggested to be related to  $\Delta h$ , because the generation of dislocations underneath the tip must accommodate the displacement of the indenter. The relation between the number of dislocation loops and pop-in width has been proposed as  $N = \Delta h / (2b)$  [37].  $b$  is the magnitude of Burgers vector, which was calculated from the lattice parameter ( $a$ ) for the studied material divided by the square-root of two as  $a/2[101]$  and equals to  $0.25$  nm [42-45].

The interaction energy between two circular prismatic dislocation loops can be expressed as [46]:

$$W_i = \frac{\mu b^2}{1-\nu} r \left( \ln \frac{8r}{d} - 1 \right) \quad (5)$$

where  $\mu$  is the shear modulus that can be determined from Poisson's ratio ( $\nu = 0.27$ ) and elastic modulus. The distance between dislocation loops  $d$  is set equal to  $b$ , if we assume the prismatic dislocation loops are continuously emitted and close-packed (Figure 3b) [38]. The radius of dislocation loops  $r$  can be estimated from the distribution of shear stress underneath the indenter shown in Figure 3c. The graphical representation of the maximum shear stress with the axis normalized to the contact radius ( $a_c = \sqrt[3]{\frac{3PR}{4E_r}}$ ) is constructed based on the Hertz-Huber model [47]. It shows that the highest value of maximum shear stress happens at the point  $0.48a_c$  below the indenter [48]. Since the maximum shear stress happens at a point, it is reasonable to estimate a region, where 98% of the maximum shear stress is acting, as the size of generated dislocation loops [20, 31]. The intersecting plane in Figure 3c defines the 98% of the maximum shear stress, and it results in a semi-elliptical region with a major half-axis of  $0.29 a_c$ , which was chosen as the radius of dislocation loop.

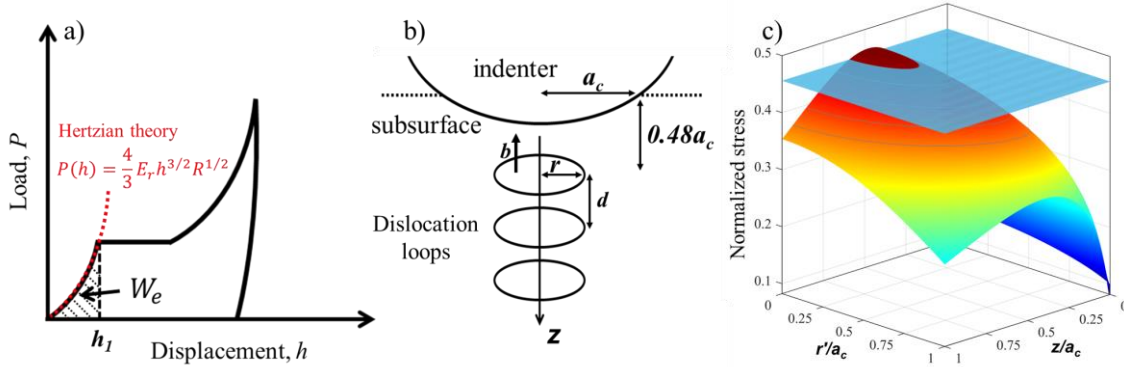


Figure 3: a) Stored elastic energy for dislocation nucleation. b) The schematic of prismatic dislocation loops beneath the indenter generated during pop-in. c) Distribution of maximum shear stress beneath the indenter according to Hertz-Huber model. The plane defines 98% of the maximum shear stress.

The total dislocation interaction energy  $W_i^t$  can be obtained by the summation over all interactions between each loop with all the rest loops, and it would give rise to the following relation [46]:

$$W_i^t = \frac{\mu b^2}{1-\nu} r \left( \left\{ \sum_{j=1}^{N-1} j \left( \ln \frac{8r}{d} \right) - \sum_{j=1}^{N-1} \ln(j!) - \sum_{j=1}^{N-1} j \right\} \right) \quad (6)$$

Also, the dislocation line energy is expressed as [49]:

$$W_s = \frac{\mu b^2}{2(1-\nu)} r \left( \ln \frac{8r}{\rho} - 1 \right) \quad (7)$$

where  $\rho$  is the radius of dislocation core and it is here equal to  $b/2$  [39]. Thus, the total dislocation line energy of  $N$  circular loops equals to  $N \times W_s$ . Therefore, the values of  $W_e$ ,  $W_i^t$ ,  $N$ , and  $W_s$  in Eq. 4 can be quantitatively calculated from the nanoindentation results. The only unknown part in Eq. 4 is the total friction energy  $W_f^t$  for dislocation motion. All the dislocation loops are assumed to be emitted from the same area beneath the indenter, followed by slipping along the indenting direction, and close-pack with a Burgers vector distance as shown in Figure 3b. Due to this, the unit friction energy  $W_f$ , as the energy for a dislocation loop to move  $b$  distance, can be expressed as  $W_f \cdot \frac{N(N-1)}{2} = W_f^t$ . The item  $N(N-1)/2$  indicates the total number of slip steps for generating  $N$  prismatic dislocation loops. By integrating Eqs. 3-7, the unit friction energy for dislocation slip in each charging condition during pop-in phenomenon can be calculated. The cumulative frequency distribution analysis [50] on unit friction energy in different conditions is shown in Figure 4. It shows that the average unit friction energy in air condition without hydrogen charging was  $1.86 \times 10^{-16}$  J, which increased to  $6.44 \times 10^{-16}$ ,  $2.79 \times 10^{-15}$ ,  $7.55 \times 10^{-15}$  J with 2.5, 14.0, and 39.6 times increment during hydrogen charging at H1, H2, and H3, respectively. When anodic discharging was applied, the average unit friction energy returned to  $2.56 \times 10^{-16}$  J, which is only 0.37 times higher than the value in air condition. The trapped hydrogen that cannot diffuse out during anodic discharging process might results in this minor remained increment.

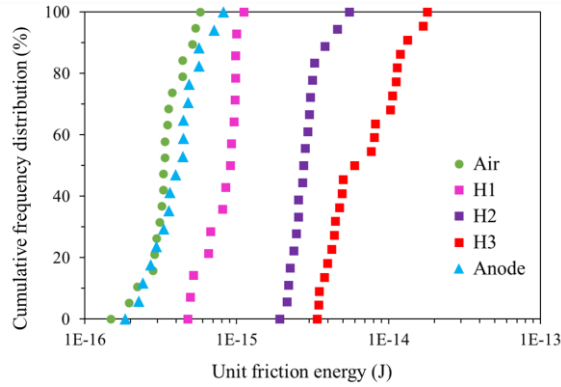


Figure 4: The cumulative frequency distribution of unit friction energy for dislocation motion at the instant of pop-in.

A very clear hydrogen-enhanced friction for dislocation motion can be concluded from Figure 4. During the pop-in process, the shear stress beneath the indenter will nucleate and drive dislocations. When hydrogen charging is applied, the hydrogen atoms are absorbed and dissolved into the subsurface of the material. On the one hand, the dissolved hydrogen enhances homogeneous dislocation nucleation through the reduction of dislocation line energy, as proposed by the former studies [21, 24], resulting in a reduced pop-in load. On the other hand, these hydrogen atoms are accumulated forming Cottrell-

like atmosphere around moving dislocations and perform substantial resistance to dislocation motion, which is consistent with the solute drag theory [14, 49, 51]. Thus, each dislocation slip step needs more energy to overcome the enhanced friction. As a result, substantial stored elastic energy will be consumed by the hydrogen-induced lattice friction and it ends up with a fewer amount of generated dislocations and a smaller pop-in width. In brief, hydrogen enhances dislocation nucleation, while impedes dislocation motion. When a higher hydrogen concentration is applied, it will enhance the induced friction, and the pop-in width is further reduced. This hydrogen-resisted dislocation motion has also been revealed by other researchers from both atomistic simulations [14, 52] and in-situ experimental studies [9, 39]. While under the anodic discharging, the dissolved hydrogen is mostly diffused out of the sample surface, and both hydrogen-induced lattice friction and hydrogen Cottrell atmosphere are eliminated. Therefore, the pop-in width is recovered to its original value in air. However, it shows that the unit friction energy in anodic condition is still slightly higher (by 0.37 times) than in air. This minor increment might be due to the relatively low amount of deep trapped hydrogen, which cannot diffuse out during anodic discharging.

In summary, the influence of hydrogen on the pop-in behavior was investigated in an equiatomic CoCrFeMnNi HEA through in-situ electrochemical nanoindentation test. The results show that hydrogen accumulatively affects the relation between pop-in width and load, where the reduction effect is more noticeable for width than load. By analyzing the interactions between hydrogen and dislocations via a comprehensive energy balance model, it was quantitatively interpreted as the enhanced lattice friction by hydrogen in consistent with the solute drag theory. As a result, fewer dislocations can be generated with a smaller pop-in width under the hydrogen charging condition. This is the first time that the intrinsic relation between hydrogen and dislocation motion related pop-in width has been quantitatively revealed, which provides unambiguous insights in the hydrogen-interrelated failure mechanisms.

### **Acknowledgements**

The authors are grateful for the support provided by Research Council of Norway through the HyLINE (294739) and M-HEAT (294689) projects. Z.L. would like to acknowledge the financial support by the Hunan Special Funding for the Construction of Innovative Province (2019RS1001).

### **Data availability**

The data that support the findings of this study are available on request from the corresponding author. The data are not publicly available as the data also forms part of an ongoing study.

## Reference:

- [1] S. Lynch, *Corros. Rev.* 30(3-4) (2012) 105-123.
- [2] A. Oudriss, J. Creus, J. Bouhattate, E. Conforto, C. Berziou, C. Savall, X. Feaugas, *Acta Mater.* 60(19) (2012) 6814-6828.
- [3] M.B. Djukic, V. Sijacki Zeravcic, G.M. Bakic, A. Sedmak, B. Rajcic, *Engineering Failure Analysis* 58 (2015) 485-498.
- [4] B. Sun, D. Wang, X. Lu, D. Wan, D. Ponge, X. Zhang, *Acta Metallurgica Sinica (English Letters)* (2021).
- [5] D. Wang, X. Lu, D. Wan, X. Guo, R. Johnsen, *Mater. Sci. Eng. A* (2020) 140638.
- [6] D. Wan, Y. Ma, B. Sun, S.M.J. Razavi, D. Wang, X. Lu, W. Song, *Journal of Materials Science & Technology* 85 (2021) 30-43.
- [7] H. Yu, A. Cocks, E. Tarleton, *J. Mech. Phys. Solids* (2018).
- [8] I.M. Robertson, P. Sofronis, A. Nagao, M.L. Martin, S. Wang, D.W. Gross, K.E. Nygren, *Metall. Mater. Trans. A* 46a(6) (2015) 2323-2341.
- [9] D.G. Xie, S.Z. Li, M. Li, Z.J. Wang, P. Gumbsch, J. Sun, E. Ma, J. Li, Z.W. Shan, *Nat. Commun.* 7 (2016).
- [10] X. Lu, D. Wang, D. Wan, Z.B. Zhang, N. Kheradmand, A. Barnoush, *Acta Mater.* 179 (2019) 36-48.
- [11] R. Kirchheim, *Scr. Mater.* 62(2) (2010) 67-70.
- [12] X. Lu, Y. Ma, D. Wang, *Mater. Sci. Eng. A* 792 (2020) 139785.
- [13] P. Ferreira, I. Robertson, H. Birnbaum, *Acta Mater.* 46(5) (1998) 1749-1757.
- [14] J. Song, W.A. Curtin, *Acta Mater.* 68 (2014) 61-69.
- [15] M.-Y. Seok, I.-C. Choi, J. Moon, S. Kim, U. Ramamurty, J.-i. Jang, *Scr. Mater.* 87 (2014) 49-52.
- [16] S. Shim, H. Bei, E.P. George, G.M. Pharr, *Scr. Mater.* 59(10) (2008) 1095-1098.
- [17] A. Barnoush, M.T. Welsch, H. Vehoff, *Scr. Mater.* 63(5) (2010) 465-468.
- [18] G. Hachet, A. Oudriss, A. Barnoush, T. Hajilou, D. Wang, A. Metsue, X. Feaugas, *Mater. Sci. Eng. A* (2020) 140480.
- [19] D. Wang, X. Lu, D. Wan, Z. Li, A. Barnoush, *Scr. Mater.* 173 (2019) 56-60.
- [20] A. Barnoush, H. Vehoff, *Acta Mater.* 58(16) (2010) 5274-5285.
- [21] D. Wang, X. Lu, Y. Deng, X. Guo, A. Barnoush, *Acta Mater.* 166 (2019) 618-629.
- [22] D. Wang, X. Lu, Y. Deng, D. Wan, Z. Li, A. Barnoush, *Intermetallics* 114 (2019) 106605.
- [23] G. Stenerud, R. Johnsen, J.S. Olsen, J.Y. He, A. Barnoush, *Int. J. Hydrog. Energy* 42(24) (2017) 15933-15942.
- [24] A. Bamoush, N. Kheradmand, T. Hajilou, *Scr. Mater.* 108 (2015) 76-79.
- [25] X. Lu, D. Wang, *Journal of Materials Science & Technology* 67 (2021) 243-253.
- [26] X. Lu, D. Wang, Z. Li, Y. Deng, A. Barnoush, *Mater. Sci. Eng. A* 762 (2019) 138114.
- [27] K.L. Johnson, *Contact Mechanics*, Cambridge University Press, Cambridge, 1987.
- [28] F. Pöhl, *Sci. Rep.* 9(1) (2019).
- [29] I. Gutierrez-Urrutia, S. Zaeferrer, D. Raabe, *Scr. Mater.* 61(7) (2009) 737-740.
- [30] Y. Zhao, J.-M. Park, J.-i. Jang, U. Ramamurty, *Acta Mater.* 202 (2021) 124-134.
- [31] A. Barnoush, *Acta Mater.* 60(3) (2012) 1268-1277.
- [32] H. Bei, Z.P. Lu, E.P. George, *Phys. Rev. Lett.* 93(12) (2004).
- [33] J.R. Morris, H. Bei, G.M. Pharr, E.P. George, *Phys. Rev. Lett.* 106(16) (2011) 165502.
- [34] D. Wu, J.R. Morris, T.G. Nieh, *Scr. Mater.* 94 (2015) 52-55.
- [35] K. Gan, D. Yan, S. Zhu, Z. Li, *Acta Mater.* 206 (2021) 116633.
- [36] C. Müller, M. Zamanzade, C. Motz, *Micromachines* 10(2) (2019) 114.
- [37] C. Shin, S. Shim, *J. Mater. Res.* 27(16) (2012) 2161-2166.
- [38] A. Gouldstone, H.J. Koh, K.Y. Zeng, A.E. Giannakopoulos, S. Suresh, *Acta Mater.* 48(9) (2000) 2277-2295.
- [39] A. Barnoush, M. Asgari, R. Johnsen, *Scr. Mater.* 66(6) (2012) 414-417.
- [40] Y. Shibutani, T. Tsuru, A. Koyama, *Acta Mater.* 55(5) (2007) 1813-1822.
- [41] K. Zhao, J. He, A.E. Mayer, Z. Zhang, *Acta Mater.* 148 (2018) 18-27.
- [42] A. Heczal, M. Kawasaki, J.L. Lábár, J.-i. Jang, T.G. Langdon, J. Gubicza, *J. Alloys Compd.* 711 (2017) 143-154.

- [43] L.R. Owen, E.J. Pickering, H.Y. Playford, H.J. Stone, M.G. Tucker, N.G. Jones, *Acta Mater.* 122 (2017) 11-18.
- [44] B. Cantor, I.T.H. Chang, P. Knight, A.J.B. Vincent, *Mater. Sci. Eng. A* 375-377 (2004) 213-218.
- [45] J.Y. He, H. Wang, H.L. Huang, X.D. Xu, M.W. Chen, Y. Wu, X.J. Liu, T.G. Nieh, K. An, Z.P. Lu, *Acta Mater.* 102 (2016) 187-196.
- [46] P.M. Anderson, J.P. Hirth, J. Lothe, *Theory of Dislocations*, 3rd ed., Cambridge University Press, Cambridge, 2017.
- [47] M.T. Huber, *Annalen der Physik* 319(6) (1904) 153-163.
- [48] W.D. Nix, H.J. Gao, *J. Mech. Phys. Solids* 46(3) (1998) 411-425.
- [49] D. Hull, D.J. Bacon, *Introduction to Dislocations*, Elsevier Science 2011.
- [50] H.P. Ritzema, *Drainage principles and applications*; 3rd ed, ILRI, Wageningen, 2006.
- [51] A.H. Cottrell, *Dislocations and plastic flow in crystals*, Clarendon Press, Oxford, 1953.
- [52] Y. Zhu, Z. Li, M. Huang, H. Fan, *Int. J. Plast.* 92 (2017) 31-44.



Dear editor-in-chief,

Thank you very much for sending us the reviewers' comments and giving us the chance to revise the manuscript. The comments from the reviewers are very constructive and valuable to us. We have implemented all the issues very carefully in the revised version and listed the responses and modifications in the "Response to Editor and Reviewer". The changes made to the original manuscript are highlighted in the "Revised Manuscript\_marked up". A clean version of the manuscript "Revised Manuscript\_clean version" containing all the changes is also prepared and attached.

Thank you very much again for your great effort to our manuscript!

Sincerely,

Xu Lu

**Declaration of interests**

The authors declare that they have no known competing financial interests or personal relationships that could have appeared to influence the work reported in this paper.

The authors declare the following financial interests/personal relationships which may be considered as potential competing interests:

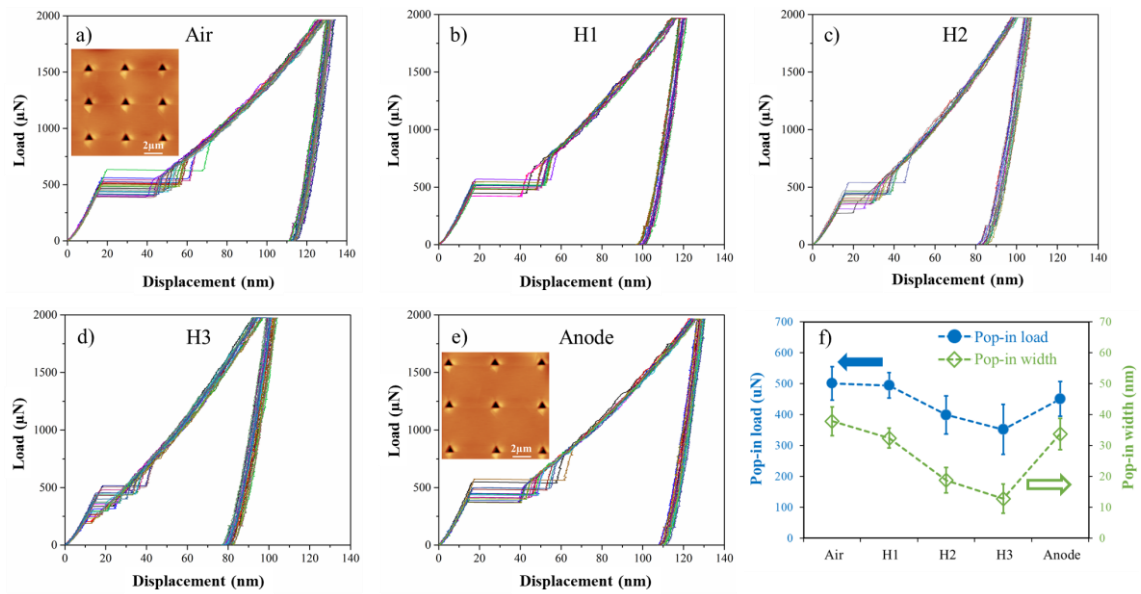


Figure 1: Load-displacement curves in (a) air, under the hydrogen charging conditions at (b) H1 (-1300 mV), (c) H2 (-1400 mV), (d) H3 (-1500 mV), and (e) anodic hydrogen discharging condition. The surface quality before and after hydrogen charging are shown as the insets in (a) and (e), respectively. (f) shows the pop-in width  $\Delta h$  and pop-in load  $p$  under different hydrogen charging conditions.

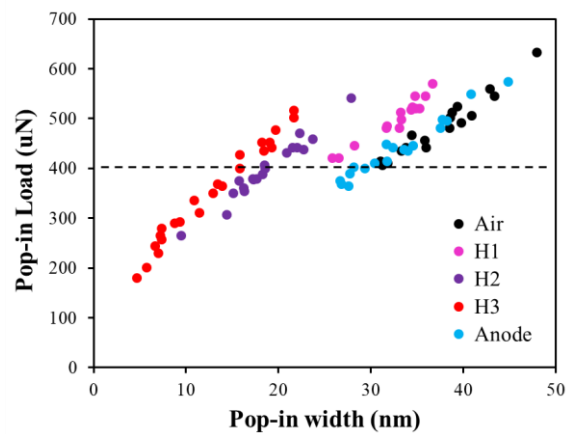


Figure 2: Relation between pop-in width and pop-in load under different hydrogen charging conditions. Dashed line shows an example of the major hydrogen effect on pop-in width.

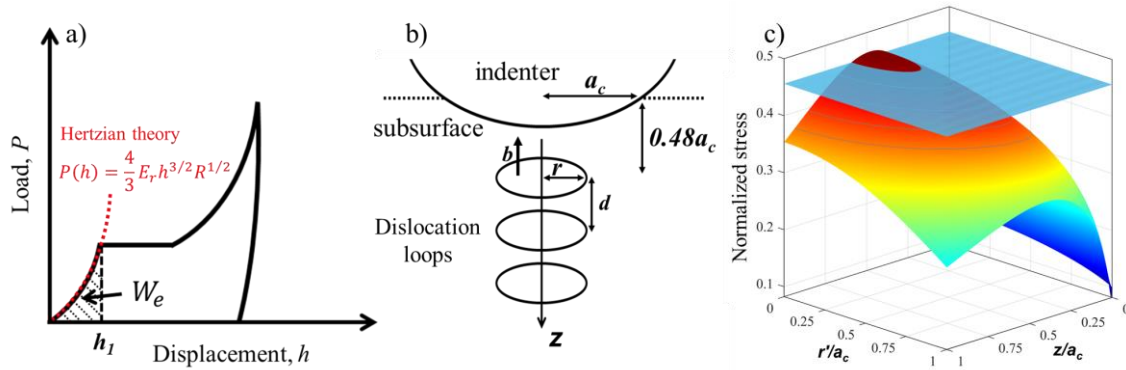


Figure 3: a) Stored elastic energy for dislocation nucleation. b) The schematic of prismatic dislocation loops beneath the indenter generated during pop-in. c) Distribution of maximum shear stress beneath the indenter according to Hertz-Huber model. The plane defines 98% of the maximum shear stress.

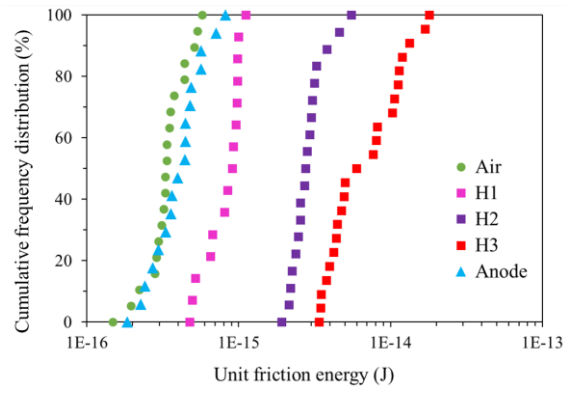


Figure 4: The cumulative frequency distribution of unit friction energy for dislocation motion at the instant of pop-in.



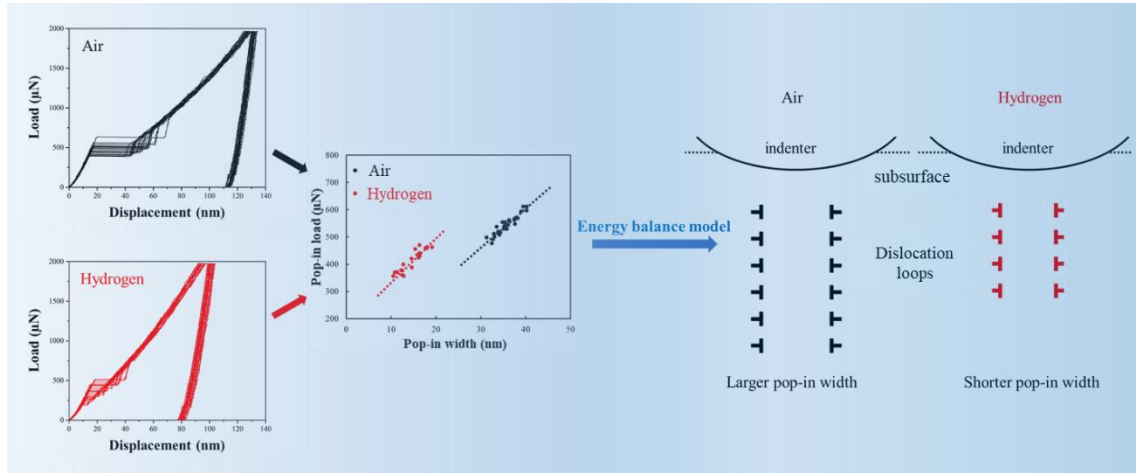
In-situ electrochemical nanoindentation test was applied on Cantor alloy.

The pop-in behavior was investigated under different H charging conditions.

Both pop-in width and load were reversibly reduced by H

The H reduction effect on pop-in width is more noticeable than that of pop-in load.

An energy balance model was used showing H reduced dislocation mobility.



## Response to Reviewer's Report

Manuscript J-MST-D-21-00421

Dong Wang, Xu Lu, Meichao Lin, Di Wan, Zhiming Li, Jianying He, Roy Johnsen

We would like to begin by thanking the editor and reviewers for the valuable comments and suggestions. The response is structured as follows: the editor's letter and the comments of the reviewers are copied below (*black, italic font*). For each comment, we present a detailed response, followed by an indication of the location of corresponding changes/modifications in the manuscript (*blue font*). The revised manuscript with all the mentioned changes is also provided, where the changes are **highlighted**.

---

### *Editor's letter:*

*Dear Dr. Lu,*

*Thank you for submitting your manuscript to Journal of Materials Science & Technology.*

*I have completed my evaluation of your manuscript. The reviewers recommend reconsideration of your manuscript following revision. I invite you to resubmit your manuscript after addressing the comments below. Please resubmit your revised manuscript by May 12, 2021.*

*When revising your manuscript, please consider all issues mentioned in the reviewers' comments carefully: please outline in a cover letter every change made in response to their comments and provide suitable rebuttals for any comments not addressed. Please note that your revised submission may need to be re-reviewed.*

*To submit your revised manuscript...*

*Journal of Materials Science & Technology values your contribution and I look forward to receiving your revised manuscript.*

*Kind regards,*

*Journal of Materials Science & Technology*

**Reviewer comments:**

**Reviewer #1:** *This study reported the pop-in behavior of an equiatomic CoCrFeMnNi high-entropy alloy under different hydrogen charging/discharging conditions by via in-situ electrochemical nanoindentation. And quantitatively revealed the pop-in width under hydrogen impact. But there are some severe problems in this article.*

**Response:** Thank you very much for the constructive comments and suggestions. The authors appreciate the reviewer for giving us the chance to improve this manuscript. We carefully addressed the comments, and the details are shown below.

(1) *"To eliminate the influence of different grain orientations, all the tests were performed in an (111)-direction grain." in this article. The question is how to ensure that every test is (111)-direction grain.*

**Response:** This point indeed would cause potential confusions for the readers, the authors thank the reviewer for pointing it out. The detailed procedures for ensuring all indents located in the same grain in the present study are summarized below:

1) **Microindents marking:** After the sample surface preparation, nine microindents were marked on the sample surface with a separation distance of 0.8-1.0 mm using 2N indenting force (Fig R1a). These microindents were used as reference points for locating the desired grain orientation using EBSD technique.

2) **EBSD:** EBSD scans covering the microindents were performed to determine the desired grain orientation (111)//ND. Fig R1b shows the chosen grain with (111) orientation marked with blue solid circle.

3) **Desired grain location determination:** The initial point for in-situ nanoindentation was determined and its distance to the center of microindent was accurately measured using SEM (Fig R1c). Moreover, the size of (111) grain was measured to get an overview of the possible test zone during nanoindentation experiment (Fig R1d).

4) **Tip-to-optical approach and in-situ nanoindentation:** During in-situ nanoindentation test, optical microscope was first focused on the microindent in Fig R1c. By using the tip-to-optical approach, the indenter tip precisely moves to the initial point on sample surface based on the distance measurements. Afterwards, the in-situ nanoindentation test was carried out on the predetermined area.

5) **Nanoindents reconfirmation:** After in-situ nanoindentation test, the sample was taken out from the cell and rinsed carefully. The tested grain was characterized by SEM to check the position of each nanoindent (Fig R1e). All the nanoindents that were located outside the grain or on the inclusions were eliminated from data analysis.

Therefore, in the current study, we guarantee that all collected data are obtained from (111) grain orientation by using the aforementioned procedures.

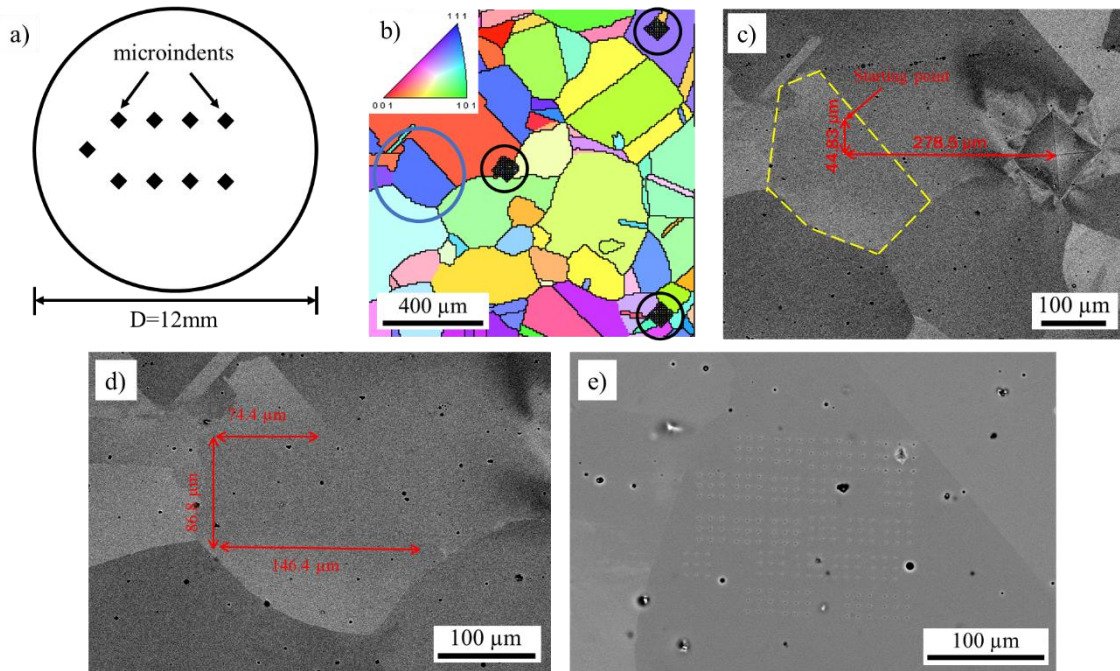


Figure R1: a) Schematic of microindent markings on the sample surface. b) ND-IPF map of the tested area. The black solid circles indicate the microindents, the blue solid circle indicates the tested (111) grain. SEM images showing c) the distance measurements for nanoindentation test (grain boundary enclosed by yellow dashed lines), d) the size measurement of the tested grain, e) the reconfirmation of the location of each nanoindents.

**Modification:** The authors added the detailed experimental procedure into the supplementary document. Also, one sentence was added to page 2 of the revised manuscript as: “The detailed experimental procedures are shown in the supplementary document.”

(2) *changing the cathode charging voltage to changing the hydrogen content, that is cannot directly characterize the hydrogen content on the surface of the material. Energy spectrum analysis should be added to characterize the hydrogen content under different voltages.*

**Response:** The authors appreciate the reviewer for this comment and suggestion. Indeed, although changing the cathodic charging potential can change the surface hydrogen concentration, it cannot directly quantify the hydrogen concentration on sample surface. Thus, to characterize the hydrogen content under different voltages, thermal desorption spectroscopy (TDS) tests were performed after each charging step. The TDS tests were performed using a hydrogen analyzer together with a mass

spectrometry detector at a constant heating rate of 25 °C/min from room temperature to 700 °C. The tested TDS curves are shown in Figure R2, and a summary of TDS results is shown in Table R1.

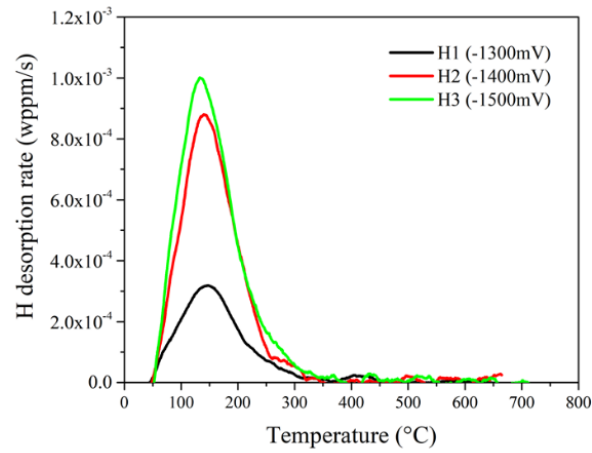


Figure R2: TDS spectra in applied cathodic charging conditions for the studied alloy.

Table R1: A summary of TDS results in applied cathodic charging conditions.

| Charging potential vs. Hg/HgSO <sub>4</sub> | Hydrogen content (wppm) | Sample thickness (mm) | Surface hydrogen content (wppm) |
|---|-------------------------|-----------------------|---------------------------------|
| -1300 mV                                    | 0.03837                 | 1.05                  | 11.76                           |
| -1400 mV                                    | 0.09558                 | 0.92                  | 25.67                           |
| -1500 mV                                    | 0.10556                 | 1.02                  | 31.43                           |

The surface hydrogen concentration  $C_s$  during different charging potential can be estimated using the method proposed by Pontini and Hermida as follows:

$$C_s = \frac{hC_M}{4} \sqrt{\frac{\pi}{Dt}} \quad (R1)$$

where  $h$  is the sample thickness,  $C_M$  is the overall hydrogen content measured by TDS,  $t$  is the charging time, and  $D$  is the hydrogen diffusion coefficient chosen as  $3.2 \times 10^{-16} \text{ m}^2/\text{s}$  [2]. As a result, the surface hydrogen contents are calculated as 11.76, 25.67, and 31.43 wppm after 2h charging at -1300, -1400, and -1500 mV, respectively.

[1] A.E. Pontini, J.D. Hermida, X-ray diffraction measurement of the stacking fault energy reduction induced by hydrogen in an AISI 304 steel, *Scr. Mater.* 37(11) (1997) 1831-1837.

[2] V. Olden, C. Thaulow, R. Johnsen, Modelling of hydrogen diffusion and hydrogen induced cracking in supermartensitic and duplex stainless steels, *Mater. Des.* 29(10) (2008) 1934-1948.

**Modification:** The authors added the calculated surface hydrogen concentration under different charging potentials to page 3 as: “Figures 1b-1d show the curves during hydrogen charging with an increasing charging potential from H1 (-1300 mV) to H3 (-1500 mV). The corresponding surface hydrogen concentrations were calculated to be 11.76, 25.67, and 31.43 wppm, respectively (detailed calculations are shown in the supplementary document)”. Moreover, the results from TDS tests and detailed calculation are summarized and added into the supplementary document.

(3). *Why the Burgers vector equals to 0.25 nm, lack of calculation formula and original data.*

**Response:** The authors thank the reviewer for pointing it out. The Burgers vector was calculated as the lattice parameter ( $a$ ) divided by the square-root of two for the studied FCC structured alloy as  $a/2\sqrt{2}$ . The lattice parameter of the studied equiatomic CoCrFeMnNi high-entropy alloy has already been reported [1, 2]. Specifically, Cantor et al. [1], performed XRD analysis on CoCrFeMnNi high-entropy alloy and reported a lattice parameter in the range of 0.358-0.364 nm. And Owen et al. performed neutron radiation on the same CoCrFeMnNi high-entropy alloy and showed a lattice parameter of 0.359 nm [2]. Therefore, by using the aforementioned calculation method, the Burgers vector equals to 0.25 nm by keeping two decimal places. Moreover, the value of 0.25 nm has been commonly used as the Burgers vector for the same CoCrFeMnNi high-entropy alloy [3-6].

[1] B. Cantor, I.T.H. Chang, P. Knight, A.J.B. Vincent, Microstructural development in equiatomic multicomponent alloys, *Mater. Sci. Eng. A* 375-377 (2004) 213-218.

[2] L.R. Owen, E.J. Pickering, H.Y. Playford, H.J. Stone, M.G. Tucker, N.G. Jones, An assessment of the lattice strain in the CrMnFeCoNi high-entropy alloy, *Acta Mater.* 122 (2017) 11-18.

[3] A. Heczal, M. Kawasaki, J.L. Lábár, J.-i. Jang, T.G. Langdon, J. Gubicza, Defect structure and hardness in nanocrystalline CoCrFeMnNi High-Entropy Alloy processed by High-Pressure Torsion, *J. Alloys Compd.* 711 (2017) 143-154.

[4] J.Y. He, H. Wang, H.L. Huang, X.D. Xu, M.W. Chen, Y. Wu, X.J. Liu, T.G. Nieh, K. An, Z.P. Lu, A precipitation-hardened high-entropy alloy with outstanding tensile properties, *Acta Mater.* 102 (2016) 187-196.

[5] N.L. Okamoto, S. Fujimoto, Y. Kambara, M. Kawamura, Z.M.T. Chen, H. Matsunoshita, K. Tanaka, H. Inui, E.P. George, Size effect, critical resolved shear stress, stacking fault energy, and solid solution strengthening in the CrMnFeCoNi high-entropy alloy, *Sci. Rep.* 6(1) (2016) 35863.

[6] J. Lee, H. Park, M. Kim, H.J. Kim, J.y. Suh, N. Kang, Role of Hydrogen and Temperature in Hydrogen Embrittlement of Equimolar CoCrFeMnNi High- entropy Alloy, *Metals and Materials International* 27 (2021) 166-174.

**Modification:** To make the Burgers vector value more reliable to readers, the authors explained the calculation method and added corresponding references to page 5 of the revised manuscript as: “ $b$  is

the magnitude of Burgers vector, which was calculated from the lattice parameter ( $a$ ) for the studied material divided by the square-root of two as  $a/2[101]$  and equals to 0.25 nm [42-45].”.

(4) *I don't quite understand the meaning of the ordinate in Fig 4.*

**Response:** The authors appreciate this question. It is important for us to ensure our manuscript can be easily understood. The ordinate in Figure 4 is cumulative frequency distribution (%). The mathematic definition of cumulative frequency distribution is “the sum of the class and all classes below it in a frequency distribution.” Taking hydrogen charging condition H3 in Figure 4 as an example, each point represents one calculated unit friction energy obtained from the corresponding load-displacement curve and can be counted as a class in the cumulative frequency analysis. A summary of unit friction energy in an ascending order under H3 condition is presented in Table R2. The cumulative frequency ( $f$ ) represents the number of energy values that lie below the unit friction energy in the corresponding row. The cumulative relative frequency ( $f/n$ ) represents the percentage of each cumulative frequency by dividing the total number of data points ( $n=21$ ). For example, there are 10 points with a value less than  $5.03037E-15$  J, and the corresponding cumulative relative frequency is 47.61905%. Thus, the cumulative frequency distribution shows an overview of all distinct unit friction energy values and their respective number of occurrences. By adopting such graphical representation, more intuitive view of hydrogen-affected unit friction energy change can be obtained.

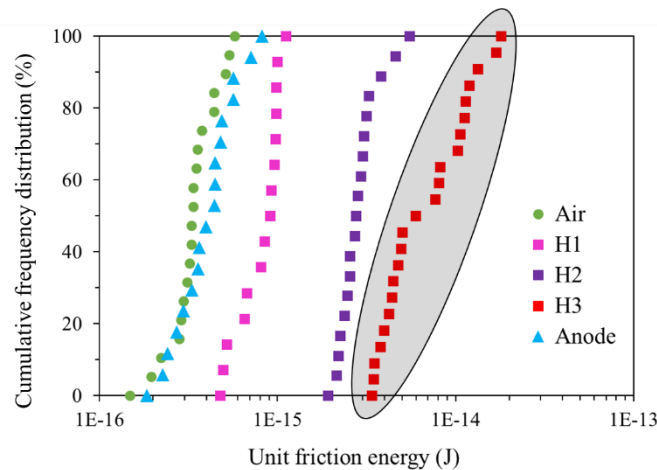


Figure R3: The cumulative frequency distribution of unit friction energy for dislocation motion. The marked area showing data under H3 charging condition.

Table R2: The unit friction energy data with its cumulative frequency distribution under H3 charging condition.

| Unit friction energy (J) | Cumulative frequency (f) | Cumulative relative frequency (f/n, %) | Unit friction energy (J) | Cumulative frequency (f) | Cumulative relative frequency (f/n, %) |
|--------------------------|--------------------------|--|--------------------------|--------------------------|--|
| 3.39274E-15              | 0                        | 0                                      | 5.96E-15                 | 11                       | 52.38095                               |
| 3.45154E-15              | 1                        | 4.761905                               | 7.6858E-15               | 12                       | 57.14286                               |
| 3.48665E-15              | 2                        | 9.52381                                | 8.07554E-15              | 13                       | 61.90476                               |
| 3.78244E-15              | 3                        | 14.28571                               | 8.1838E-15               | 14                       | 66.66667                               |
| 3.9481E-15               | 4                        | 19.04762                               | 1.02529E-14              | 15                       | 71.42857                               |
| 4.21905E-15              | 5                        | 23.80952                               | 1.06345E-14              | 16                       | 76.19048                               |
| 4.39435E-15              | 6                        | 28.57143                               | 1.11786E-14              | 17                       | 80.95238                               |
| 4.4507E-15               | 7                        | 33.33333                               | 1.13469E-14              | 18                       | 85.71429                               |
| 4.73098E-15              | 8                        | 38.09524                               | 1.19462E-14              | 19                       | 90.47619                               |
| 4.94E-15                 | 9                        | 42.85714                               | 1.33338E-14              | 20                       | 95.2381                                |
| <b>5.03037E-15</b>       | <b>10</b>                | <b>47.61905</b>                        | 1.68414E-14              | 21                       | 100                                    |

**Modification:** The authors emphasized the ordinate of Figure 4 in page 7 of revised manuscript with an added reference.

**Reviewer #2:** *The authors presented their discussion on the observed decrease in pop-in width of hydrogenated a FCC metal during in-situ nanoindentation experiments in a short letter. With a smart in-situ nanoindentation experiment under electrochemical hydrogenation/dehydrogenation environment, they observed decrease in pop-in load and pop-in width which were also consistently observed in a TWIP steel on their previous publication (Acta Mater. 2019). On this short letter, they made a simple model explaining the decrease in pop-in width which is the novel contribution of this letter. Although further discussion and debate would be necessary for the micro-scale hydrogen interaction with dislocations, the model proposed appears reasonable and deserves attention of the researchers in the field. The manuscript is well written that it is easy to read and leads to a meaningful result. Therefore, the publication of the manuscript is recommended.*

**Response:** The authors appreciate the positive feedback and support from the reviewer. Indeed, elaborated discussion and debate are necessary to better reveal the micro-scale interaction between hydrogen and dislocations. The authors are working on a study including different types of FCC materials (Ni-based superalloys, TWIP steel, 316 stainless steel, and Cantor alloy) and discussing the hydrogen effect on elastic modulus, dislocation nucleation and motion, and hardness via combined in-situ small-scaled experimental and simulation approaches. It will provide more comprehensive understanding of the interrelation between hydrogen and dislocations.